LA-UR-99-4679
This paper has been submitted to 'Journal of Geophysical Research Atmospheres'.

Geolocation of recurrent-emission lightning storms using the FORTE satellite

Paul E. Argo
Abram R. Jacobson
Stephen O. Knox

Space and Atmospheric Sciences Group
Los Alamos National Laboratory
Los Alamos, NM 87545

ABSTRACT

The FORTE satellite, launched 29 August 1997, carries three radio-frequency-receivers for the study of lightning. Among the many interesting phenomena observed in the FORTE database are what we have termed "recurrent-emission storms." A majority of the RF events detected by the FORTE satellite are part of these recurrent-emission storms. The data are best described as coming from a single VHF emission center (the storm) which radiates to FORTE recurrently during the overhead passage of the satellite (a given ground point is visible for approximately 15 minutes for a directly overhead passage). Closer examination reveals that the recurrently emitting storm is typically made up of emission pulses that radiate many times within single flashes, as well as recurrent flashes that occur throughout the duration of the FORTE overflight. By exploiting dispersive propagation effects and measuring the time separations between the direct and reflected pulses (for the so-called trans-ionospheric pulse pairs or TIPPs events), we can estimate the location of the recurrent emission centers including source altitudes.

1. Introduction

Electromagnetic emissions from lightning cover most of the radio frequency spectrum as well as the visible light spectrum. This paper will discuss observations of lightning in the lower range of the Very High Frequency (VHF) radio band (28 - 48 MHz) made by the FORTE (Fast On-orbit Recording of Transient Events) satellite. The FORTE satellite was designed to be maximally sensitive to very short duration(few microsecond) impulsive events, especially with its multi narrow-band receivers (for a complete system description see the papers by Enemark and Shipley, 1994 and Jacobson et al, 1999). In the fourteen months since launch, this satellite has detected nearly two million transient RF events.

Jacobson, et al (1999) have shown that many of the events detected by FORTE are a pair of dispersed narrow pulses that we refer to as Trans-Ionospheric Pulse Pairs, or TIPPs. The observations are consistent with the interpretation that FORTE is observing an initial pulse from an elevated source and a subsequent ground reflection. Unlike the so-called 'hard' TIPPs seen by the Blackbeard instrument on the ALEXIS satellite (Massey and Holden, 1995; Massey et al, 1998), most of these pulses have very little energy above 100 MHz. Massey et al showed that the hard TIPPs must be generated by very localized sources (a few meters). We believe the FORTE soft TIPPs are generated by larger, but still small (hundreds of meters) (see Smith et al, 1999) discharge regions. These are therefore very unlike the historic lightning emissions observed from both cloud-to-ground and intra-cloud strokes.

If any of the lightning processes have significant impulsive events imbedded within their emissions, the FORTE rf system has the opportunity to detect them. The FORTE satellite does observe broadband rf signals that extend over hundreds of microseconds and that we believe are caused by cloud-to-ground and intra-cloud activity (Jacobson, 1999). In most of these cases we are able to de-chirp the impulsive parts of the signal, and hence determine the characteristics of the signal propagation through the ionosphere (Jacobson, 1999).

Although the FORTE satellite is unable to geolocate individual pulses, when an ensemble of pulses from a single recurrent emission storm is examined it is often possible to identify the general area in which the lightning occurs. By making use of dispersive propagation effects on the pulse and measuring the time separations between the direct and reflected pulses (for TIPP events), we can estimate the location of the recurrent emission centers including source altitudes. In this paper we will describe the models that allow us to perform this location process, and will present examples of geolocated storm centers.

2. TEC Calculations

The canonical equation for total electron content (TEC) calculations (from Massey et al, 1998) is

$$\tau_g = R/c + \alpha N_e/(f + f_c \cos(\beta))^2 + O(f_p/f)^4$$

where α=1.34x10^7 when all quantities are expressed in mks units, and N_e is the total integrated density of electrons along the path, β is the angle between the wave vector and the magnetic field, and f_c is the electron cyclotron frequency. For each frequency,

$$\Delta t = \tau_g - \tau_0 \quad \alpha N_e/(f \pm f_e \cos(\beta))^2$$

We determine the value of N_e by fitting a $1/f^2$ curve to the measured delay data, in essence ignoring higher order terms in the expansion. This approximation works well for relatively low electron densities and steep angles of incidence. But when the incidence angles are within about 45 degrees to the horizon, and electron densities are high, the ignored higher order terms resulting from refractive bending begin to have a significant effect.

3. TEC versus distance

The actual measured TEC is a combination of the vertical incidence integrated electron content from the ground to the satellite, and the angle of the signal path through the ionosphere. In a simple slab ionosphere (ignoring refraction) this can be approximated as $N_e^{vertical}/\cos(\delta)$ where δ is the zenith angle. From spherical geometry, $\cos(\delta_{300}) = R_e/(R_e+300) * \cos(\delta_0)$, where δ_0 is the zenith angle at the ground, and δ_{300} is the angle at 300 kilometer height (nominally the height of the layer maximum). A model of the TEC variation with the ray angle can be approximated as: $N_e^{vertical}/\cos(\delta_{300})$, as long as refractive effects of the raypath can be ignored. Using simple geometry we can relate the ray angle to the distance between the lightning source and the satellite position. Finally, the variation of the distance between the source and the satellite track is parameterized to the closest approach (miss) distance between the source location and the satellite track.

We also used a three dimensional raytrace code, TRACKER (Argo et al, 1992), to more accurately model the changes in the dispersion curve both as a function of the distance of the sub-satellite point from the source, and for high and low instances of the ionospheric density. The use of low- and high-density ionospheric models allows us to determine the effects that day/night conditions might have on our locating capabilities. Figure 1 shows the calculated TEC for several miss distances (closest approach of the satellite to the source) for both high- and low-density ionospheres. Since in general we know neither the miss distance nor the vertical TEC for a given TEC data set, in both cases the TEC curves are normalized to the minimum observed TEC. As expected, the TEC increases as the satellite moves further from its closest miss distance. The low-density ionosphere also has a lower rate of change of TEC with miss distance than the higher density ionosphere, a fact not accounted for in the simple model. These differences are due to two main effects: 1) the low-density (nighttime) ionosphere is higher in altitude (so the 300 kilometer height assumption breaks down) and is not so thick, and 2) the daytime

ionosphere is dense enough that significant refraction may be occurring in the wings of the curves. Since the lower density ionosphere leads to distinctly less curvature in the TEC versus down-track distance, it is important to keep track of the minimum TEC for each curve, and use either the low- or high-density model as indicated. The relationship of curvature to closest miss distance can be inverted and used to estimate distance, after the curvature has been measured experimentally. Figure 1 shows this relationship between curvature and miss distance for the modeled data.

Figure 1: Normalized curves of TEC versus satellite location along the path, as measured from the closest miss point. The TEC values at each distance have been normalized to the minimum TEC measured on the curve, since we will know neither the miss distance nor the ionospheric vertical TEC values on collected data. The TRACKER raytrace program was used with both high- and low-density ionospheric models to give the solid and dashed curves. The low-density ionosphere (nighttime) is shown in dotted curves, and has less curvature. The important feature is that the curvature of these curves is dependent upon the closest approach distance, although there is also a functional dependence on the ionospheric density.

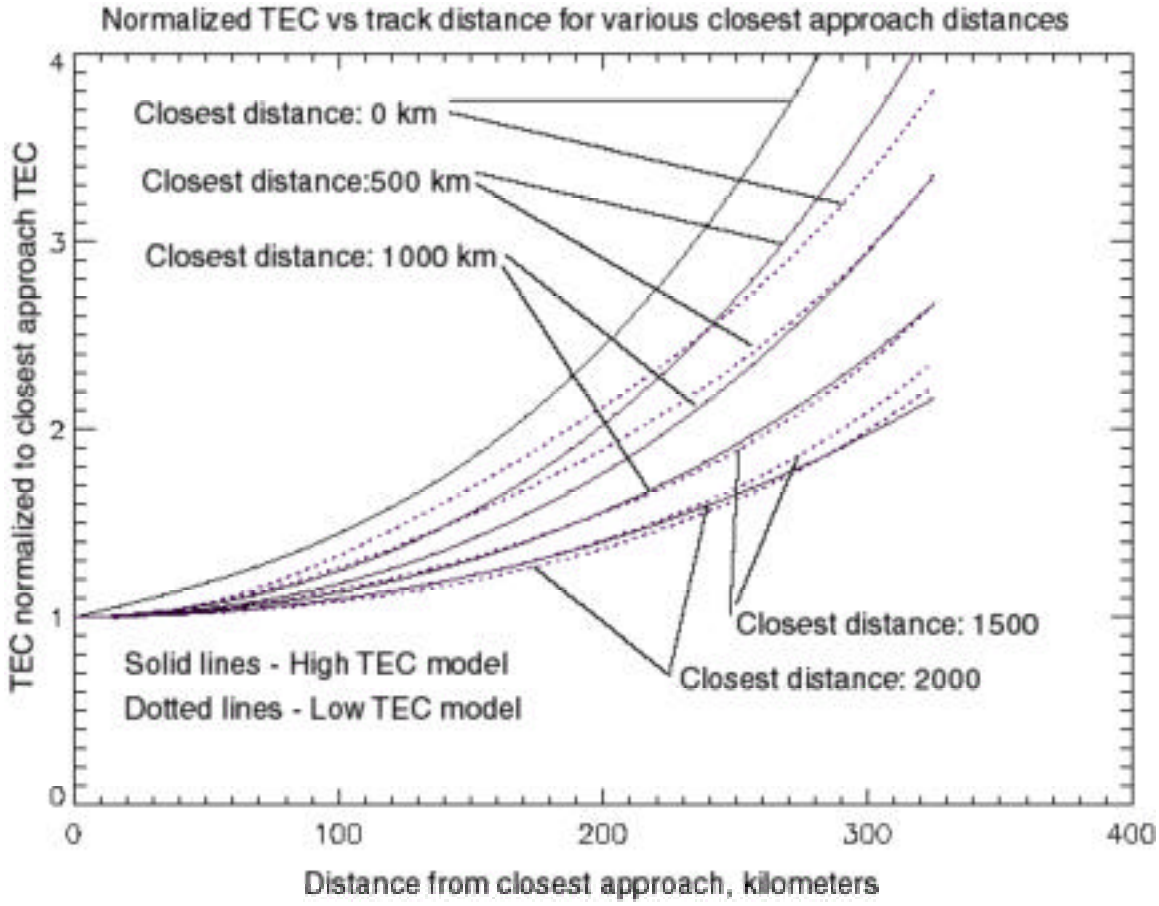

In order to validate the model, we used data from the FORTE satellite as it passed by the Los Alamos Portable Pulser. This pulser has been described previously (Smith et al, 1997; Massey et al, 1998); it is important to point out here that the pulser generates very powerful, short duration(nanoseconds) pulses that illuminate the FORTE satellite as it passes overhead. Using data from many of these passes, for many closest miss distances and differing ionospheric conditions, we can compare the measurements of the curvature to the presented model. The data points presented in Figure 2 are those calibration points. Figure 3 shows the comparison of actual miss distances to calculated distances for the pulser data. Most errors are within a few hundred kilometers, although occasionally the miss is nearer 500 km.

Figure 2: The modeled quartic curvature of the curves from Figure 2 (both high- and low-density ionospheres), as a function of miss distance. The asterisks show calibrations from the Los Alamos Portable Pulser.

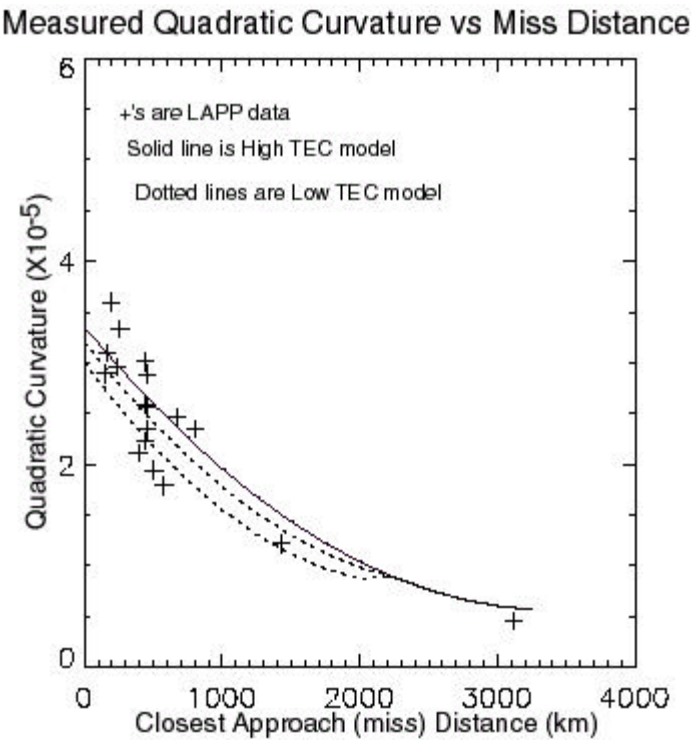

Figure 3 shows the comparison of actual miss distances to calculated distances for the pulser data. Most errors are within a few hundred kilometers, although occasionally the miss is nearer 500 km.

Figure 3: Comparison of the actual miss separation to the estimated miss separation using the models shown if Figure 3. The data points are from individual sets of data gotten by emitting a sequence of narrow pulses at the FORTE satellite as it passed by Los Alamos

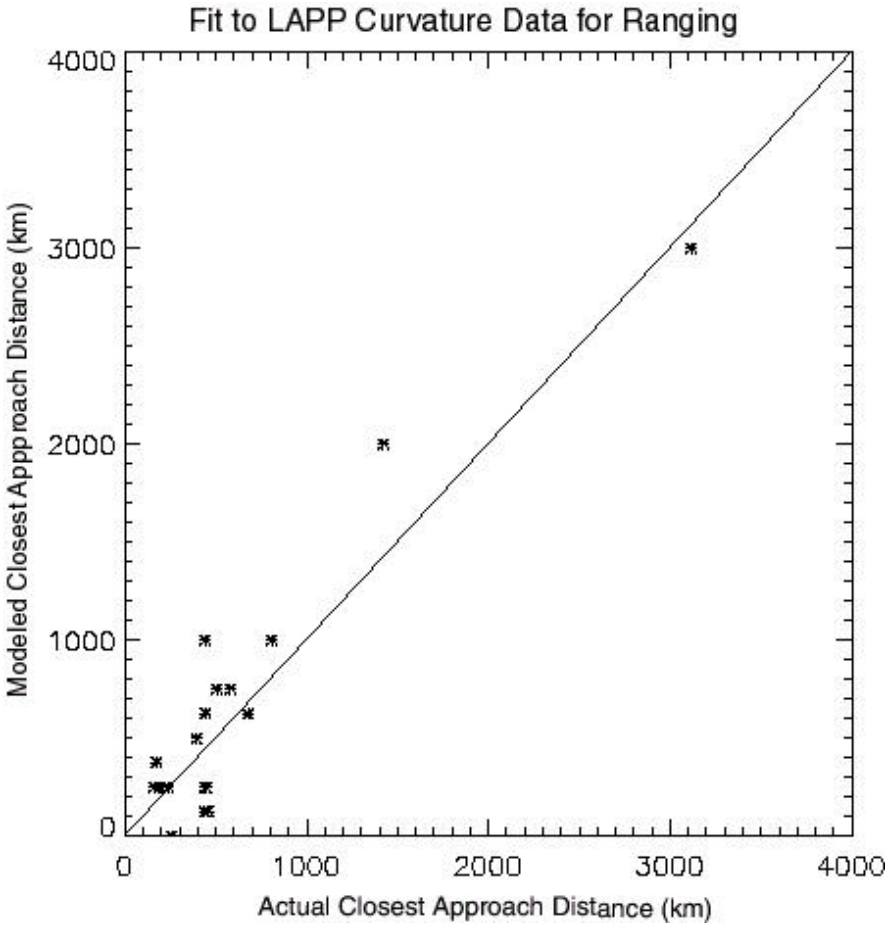

3.1 Ionospheric Gradients

The above TEC modeling was done assuming that the ionosphere was spherically symmetrical and that no horizontal gradients existed. We know that there are always horizontal gradients in the ionosphere, especially in the equatorial regions where we find most thunderstorms. In specific cases (Massey et al, 1998) we have shown that inputting

realistic ionospheres into the TRACKER model (Argo et al, 1992) will match the measured TEC variations along the path, even when there are strong horizontal ionospheric gradients present. We intend to include a simplified version of this capability in future studies, but for this study we simply ignored data showing strong asymmetries in the TEC curves.

4. TIPP separation modeling

In this section we predict more quantitatively the implications of the ground reflection model on the intra-TIPP lag in order to set the stage for approximate geolocation of recurrent-TIPP storms using the TIPP separation characteristics. Figure 4 shows the geometry for the ground reflection model. A VHF emitter ("*e*") is located in the lower atmosphere, at height *a* above the ground. A satellite ("*s*") is at an altitude *h* above its nadir point on the ground ("*n*"). The angle between *n* and *e* is θ. The arclength on the surface of the Earth, between *n* and *e*, is θR_E, where R_E is the Earth radius. In the following text we will assume both that $a << h$ and $\theta^2 << 1$. The former is guaranteed by the fact that the troposphere extends only to ~15 km, while the satellite is at ~800 km. The latter is true because the very horizon seen by FORTÉ is at only $\theta_{max} = 0.5$ radian, and most of the data we treat will be from emitters much closer to the nadir than the horizon.

Figure 4: Cartoon to show the geometry leading to the TIPP events A VHF emitter is located at a height "a" above the ground. Both a direct and ground reflected pulse reach the satellite at altitude "h".

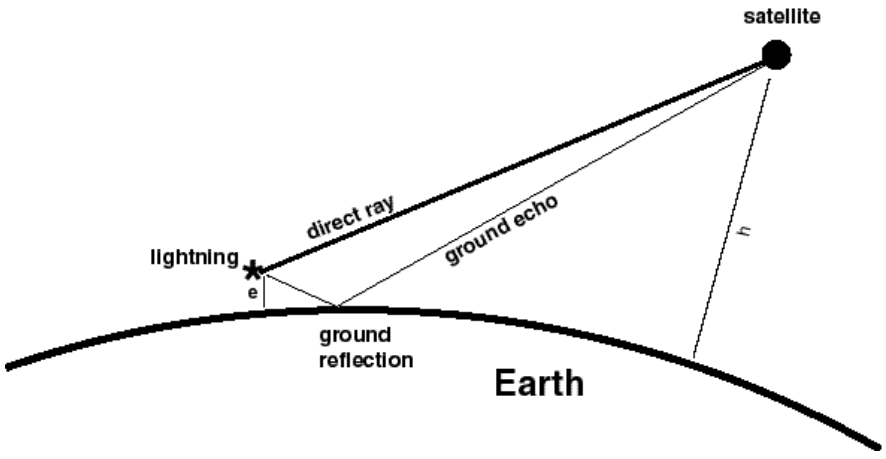

From the emitter, the satellite elevation angle is θ. Figure 4 shows that

$$\tan\{\theta + \beta\} = \frac{h + R_E(1 - \cos\theta)}{R_E \sin\theta}$$

from which it follows that

$$\beta = \text{atan}\{ [h + R_E (1 - \cos\theta)] / R_E \sin\theta \}$$

Jacobson et al (1999) have shown that the increased path length of the reflected signal (figure 4) is **p – q,** which can be shown to be:

$$\mathbf{p - q} = a/\sin(\beta) * \{1 - \cos(2\beta)\}$$

where *a* is the emitter height and β is the satellite elevation angle. If τ is the intra-TIPP time separation, then the emitter height, a, can be described as:

$$a = c\tau \sin(\beta)/ (1 - \cos(2\beta)) \qquad (1)$$

where c is the speed of light. This equation is useful if we know the horizontal location (latitude and longitude) of the emitter, but in the case of a recurrent-emitter overflight we must use the fact that equation (1), by holding *a* constant, describes a family of curves corresponding to different miss distances, or to different arc-separations from the emitter at closest approach by the satellite. Each member of the curve family has a shape depending solely on the miss distance, *even when normalized to its own peak value*. For a satellite path directly over the emitter (miss distance = 0), the curve's normalized curvature is strongest, while for the satellite almost on the horizon at closest approach (miss distance approaching the radius of the horizon small circle, or 3200 km), the normalized curvature is weakest. Figure 5 shows the separately normalized theoretical curves from inverting Eq. (1) to get τ in terms of β. These curves can be used to match the data arising from discharges *at the capping altitude* – some data will appear well below the curves, corresponding to VHF radiation from altitudes lower than the capping altitude.

Figure 5: Family of curves gotten by solving the TIPP separation model for various source heights.

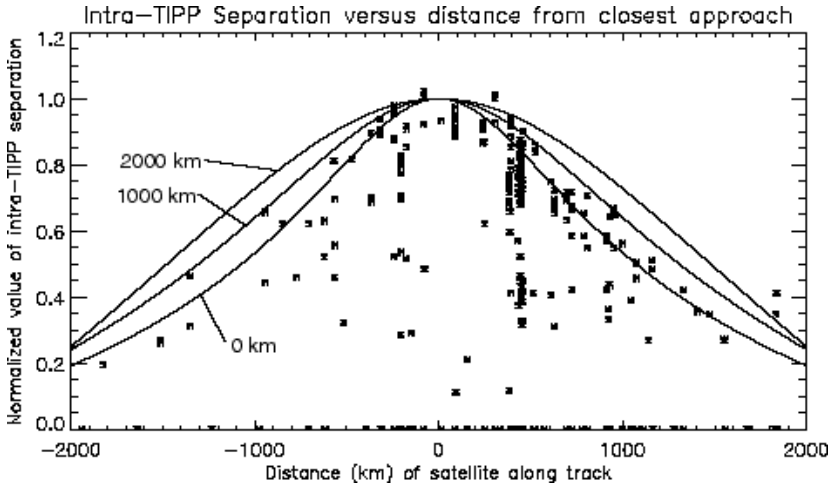

5. Geolocation examples

As the FORTE satellite passes within view of a thunderstorm, it may detect a series of impulsive lightning events whose TEC curvature and TIPP separations follow the above models. In this section we will show three examples of these storm passages, and how the satellite data provides information on the location of the source thunderstorm.

In these cases we also use a composite infrared image of the earth (in the 11.5 to 12.5 um band), showing the locations of cold cloud systems. These images are obtained from the University of Wisconsin-Madison Space Science and Engineering Center. An example is shown in figure 6a.

In Figure 6a the satellite track during data acquisition can be seen as the thick black line crossing Mexico. The asterisk at the top indicates the starting position of the data acquisition. The black asterisk to the left of the track indicates the final position of the storm location determination. Figure 6b shows the TIPP separations for the lightning data, with a maximum separation of about 80 μseconds. Figure 6c shows the TEC values fit to the lightning data. The solid curve is the best fit model for the curves, from the specified source position. The minimum TEC value is determined by the data. In both Figures 6b and c the small dots are the measured data, and the larger dots are those that lie close to the “best-fit” TEC curve. Note that along the satellite track there are several other storm cloud systems that appear to not have significant lightning associated

with them. The TEC curve data show some of the slight asymmetries that occur as a result of the propagation effects, presumably because the ionosphere is not constant along the path. In addition, the TIPP separation data appears slightly offset from the TEC curve, again probably due to slight gradients in the ionospheric electron densities.

Figure 6: Data from a recurrent emission storm detected at 13:55UT on November 20, 1998. The located storm is off the western coast of Central America. Notice that most of the cloud systems the satellite passes do not generate lightning emissions as seen from FORTE. Figure 6b shows the measured TIPP separations. Figure 6c shows the TEC measurements. The larger asterisks are the data believed to be associated with the identified storm system.

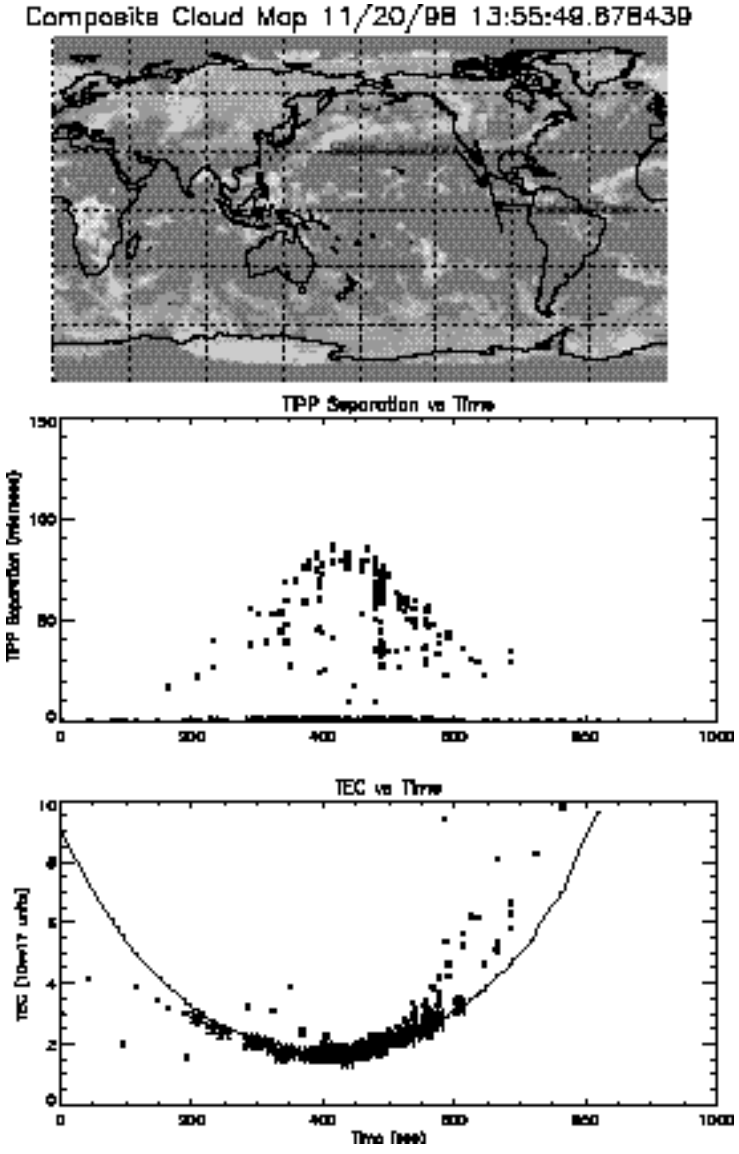

Figure 7a shows another determination of a localized lightning producing storm. In this case it appears that only the tip of the extended storm was responsible for the lightning. This is often not the situation, and much of the time the data of measured TEC versus time does not show easily separable storm curves. Notice again that most of the storm systems within view during the satellite passes appear to have no lightning associated with them, or are at least not recorded by the FORTE instruments.

Figure 7: Similar to Figure 6, but for a storm located off the Western coast of Africa at 08:31UT on November 21, 1998. Again, several cloud systems were passed with little indication of lightning activity.

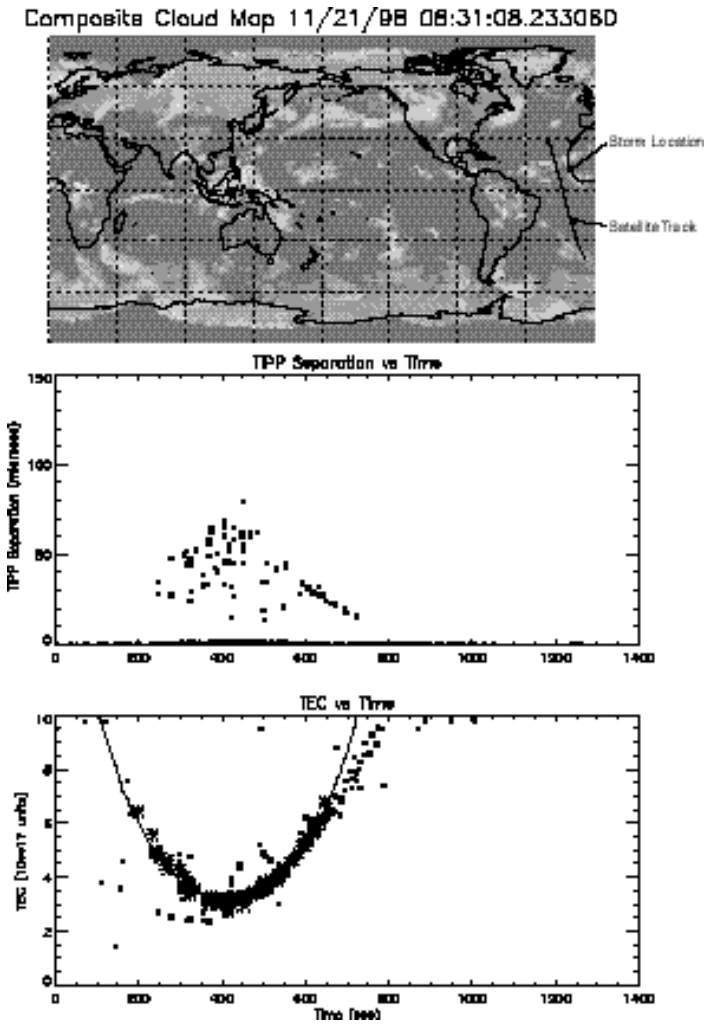

Figure 8 is similar in content to Figures 6 and 7, showing passage of the FORTE satellite by a strong lightning-producing storm. In this case, however, there are also lightning events detected that are apparently not connected to the identified and located storm system. In fact, the main storm is near the center of the satellite track, while a series of lightning events seem to come from the later parts of the path. These flash events show series of stroke events with several impulse detections in a very short time (usually a fraction of a second), and with separations of several to several tens of seconds between sets. These have been identified as flashes, and will be discussed in future papers. It should be noted that the TIPP separations of these flashes tend to cover an extended range, indicating that the emissions are coming from an extended altitude range within the cloud.

In the three storm examples described above, the TIPP separations were consistent with discharge processes occurring between several kilometers and up to about 15 kilometers in altitude. In some storm cases the discharges appear to occur at a very consistent altitude, with the TIPP separation data lying along a curve similar to the model shapes. It is not clear what causes these storm to storm differences.

Figure 8: A recurrent storm observed I the mid-Pacific at 13:55UT on July 2, 1998. Note that in this case, as opposed to those in Figures 6 and 7, there are indications of lightning activity not associated either with the identified storm system, or in fact any other isolated storm. In this data we show "flash" data, where several impulsive emissions are detected within a fraction of a second. In most of these cases the flash shows large altitudinal extent.

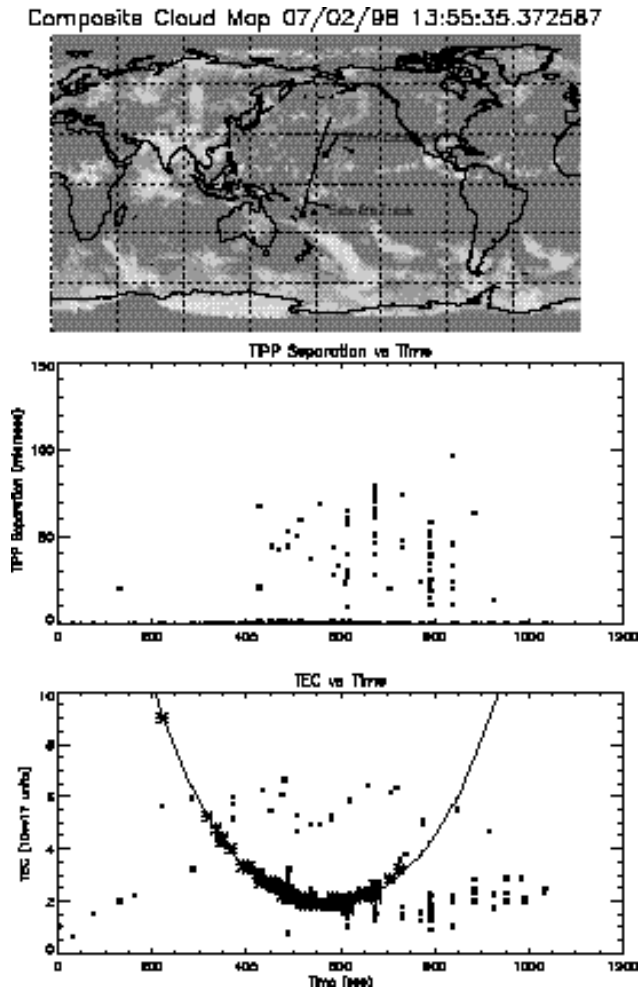

6. Conclusions

Although FORTE cannot determine the location of individual lightning events, it is often possible to exploit the information available in the ensemble of flashes that a recurrent-emission storm produces. Both the character of the dispersion curvature and the time delays measured between the direct pulse and its ground reflection can be modeled.

We have shown three separate storm passages in which we were able to isolate the lightning events and connect them to that specific storm. In all cases we used satellite infrared imagery to identify potential source regions. In many cases it is possible to use all this information and locate the storm (to within a few hundred kilometers).

In future work we will be using this ability to geolocate storms and study various aspects of thunderstorms. We intend to provide maps showing the location of occurrences of thunderstorms, perhaps with seasonal dependencies. We will be able to identify storm systems that have large amounts of lightning and do comparative investigations of the characteristics of these storms with the non-lightning emission storms.

Acknowledgement

This work was performed under the auspices of the United States Department of Energy. The authors would like to thank the members of the FORTE engineering team, the FORTE operations team, and the FORTE software/data team for making this work possible. Innumerable conversations with members of the FORTE science team have been instrumental in the understanding of the masses of FORTE data. We would also like to thank the University of Wisconsin-Madison, Space Science and Engineering Center for providing the global composite infra-red maps.

References

Argo, P., J. Fitzgerald, and R. Carlos, NICARE I HF propagation experiment results and interpretation, *Radio Science*, **27**, 289-305,1992

Enemark, D.C., and M.E. Shipley, The FORTE receiver and sub-band triggering unit, in Eighth Annual American Institute of Aeronautics and Astronautics (AIAA)/ Utah State University (USU) Conference on Small Satellites, Utah State University, Logan, Utah, 1994.

Jacobson, A.R., K.L. Cummins, M. Carter, P. Klingner, D. Roussel-Dupre, S.O. Knox, FORTE observations of lightning radio-frequency signatures: Prompt coincidence with National Lightning Detection Network sferics, submitted to *J. Geophys. Res.*, 1999

Massey, Robert S., Stephen O. Knox, Robert C. Franz, Daniel N. Holden, Charley T. Rhodes, Measurements of trans-ionospheric propagation parameters using the FORTE satellite, submitted to *Radio Science*, 1998

Smith, D.A., D.M. Delapp, D.N. Holden, G.L. Stelzter, and P.L. Klingner, Calibration and evaluation of Blackbeard time tagging capability, 11th Annual AIAA/USU Conference on Small Satellites, IF-6, Utah Statue University, Logan, Utah, 1997

D. A. Smith, X. M. Shao, D. N. Holden, C. T. Rhodes, M. Brook, P. R. Krehbiel, M. Stanley, W. Rison, R. J. Thomas, Distinct, Isolated Thunderstorm Radio Emissions, accepted JGR, 1998

Figure Captions

Figure 1: Normalized curves of TEC versus satellite location along the path, as measured from the closest miss point. The TEC values at each distance have been normalized to the minimum TEC measured on the curve, since we will know neither the miss distance nor the ionospheric vertical TEC values on collected data. The TRACKER raytrace program was used with both high- and low-density ionospheric models to give the solid and dashed curves. The low-density ionosphere (nighttime) is shown in dotted curves, and has less curvature The important feature is that the curvature of these curves is dependent upon the closest approach distance, although there is also a functional dependence on the ionospheric density.

Figure 2: The modeled quartic curvature of the curves from Figure 2 (both high- and low-density ionospheres), as a function of miss distance. The asterisks show calibrations from the Los Alamos Portable Pulser.

Figure 3: Comparison of the actual miss separation to the estimated miss separation using the models shown if Figure 3. The data points are from individual sets of data gotten by emitting a sequence of narrow pulses at the FORTE satellite as it passed by Los Alamos.

Figure 4: Cartoon to show the geometry leading to the TIPP events A VHF emitter, at “e’, is located at a height *a* above the ground. Both a direct and ground reflected pulse reach the satellite “s” at altitude “h”.

Figure 5 Family of curves gotten by solving the TIPP separation model for various source heights

Figure 6: Data from a recurrent emission storm detected at 13:55UT on November 20, 1998. The located storm is off the western coast of Central America. Notice that most of the cloud systems the satellite passes do not generate lightning emissions as seen from FORTE. Figure 6b shows the measured TIPP separations. Figure 6c shows the TEC measurements. The larger asterisks are the data believed to be associated with the identified storm system.

Figure 7: Similar to Figure 6, but for a storm located off the Western coast of Africa at 08:31UT on November 21, 1998. Again, several cloud systems were passed with little indication of lightning activity.

Figure 8: A recurrent storm observed I the mid-Pacific at 13:55UT on July 2, 1998. Note that in this case, as opposed to those in Figures 6 and 7, there are indications of lightning activity not associated either with the identified storm system, or in fact any other isolated storm. In this data we show “flash” data, where several impulsive emissions are detected within a fraction of a second. In most of these cases the flash shows large altitudinal extent.